Title
Probing the Organic-Mineral Interface at the Molecular Level in Model Biominerals

Authors
Metzler, Rebecca A.
Kim, Il Won
Delak, Katya
et al.

Publication Date
2008-03-15

PROBING THE ORGANIC-MINERAL INTERFACE AT THE MOLECULAR-LEVEL IN MODEL BIOMINERALS

Rebecca A. Metzler[1], Il Won Kim[2], Katya Delak[2], John Spencer Evans[2], Dong Zhou[1], Elia Beniash[3], Fred Wilt[4], Mike Abrecht[5], Jau-Wern Chiou[6], Jinghua Guo[7], Susan N. Coppersmith[1], P.U.P.A. Gilbert[1,]*

[1]*Department of Physics, University of Wisconsin–Madison, 1150 University Avenue, Madison, WI 53706.*

[2]*Center for Biomolecular Materials Spectroscopy, Laboratory for Chemical Physics, New York University, 345 E. 24th Street, New York, NY 10010.*

[3]*Deptartment of Biomineralization, The Forsyth Institute, 140 The Fenway, Boston, MA, 02115-3799.*

[4]*Department of Molecular and Cell Biology, University of California–Berkeley, Berkeley, CA 94720-3200.*

[5]*Synchrotron Radiation Center, 3731 Schneider Drive, Stoughton, WI 53589, USA.*

[6]*Department of Applied Physics, National University of Kaohsiung, Kaohsiung 81148, Taiwan.*

[7]*Advanced Light Source, Lawrence Berkeley National Lab, Berkeley, CA 94720.*

**Previously publishing as Gelsomina De Stasio. Corresponding author: pupa@physics.wisc.edu*

ABSTRACT. It is widely known that macromolecules, such as proteins, can control the nucleation and growth of inorganic solids in biomineralizing organisms. However, what is not known are the complementary molecular interactions, organization, and rearrangements that occur when proteins interact with inorganic solids during the formation of biominerals. The organic-mineral interface (OMI) is expected to be the site for these phenomena, and is therefore extraordinarily interesting to investigate. In this report we employ x-ray absorption near edge (XANES) spectromicroscopy to investigate the electronic structure of both calcium carbonate mineral crystals and polypeptides, and detect changing bonds at the OMI during crystal growth in the presence of polypeptides. We acquired XANES spectra from calcium carbonate crystals grown in the presence of three mollusk nacre-associated polypeptides (AP7N, AP24N, n16N) and in the presence of a sea urchin spicule matrix protein, LSM34. All these model biominerals gave similar results, including the disruption of CO bonds in calcite, and enhancement of the peaks associated with C–H bonds and C-O bonds in peptides, indicating ordering of the amino acid side chains in the mineral-associated polypeptides and carboxylate binding. This is the first evidence of the mutual effect of calcite on peptide chain, and peptide chain on calcite during biomineralization. We also show that these changes do not occur when Asp and Glu are replaced in the n16N sequence with Asn and Gln, respectively, demonstrating that carboxyl groups in Asp and Glu do participate in polypeptide – mineral molecular associations.

KEYWORDS. Biomineral, model biomineral, organic, interface, molecular ordering, XANES, X-PEEM.

INTRODUCTION

Biomineralization, or the formation of inorganic phases by living organisms, is a widespread and important phenomenon in Nature.[1-3] Biominerals serve a number of useful purposes in organisms, such as mechanical support and protection, gravity and magnetic perception, light amplification and transmission, and/or metabolic energy generation. The diversity in function is also matched by the diversity in form: over 60 different forms of biominerals exist in natural systems, and include members of the oxides, sulfides, carbonates, phosphates, oxalates and silica families. What interests the broad scientific community is that the structure and formation of biominerals are controlled over different length scales by macromolecules such as proteins, lipids, glycoproteins and polysaccharides. [1-3] In some cases, these processes lead to the formation of composite structures that incorporate macromolecules on or within the mineral phases themselves. Materials scientists are striving to understand how to synthesize composite materials that outperform their individual constituents, while in Nature such remarkable materials have evolved since the Cambrian, for more than 500 million years. [4] A striking example is nacre, or mother-of-pearl: this is a layered composite of proteins and aragonite, 3000 times more resistant to fracture than aragonite alone. [5] Sea urchin skeletal elements, comprised of single calcite crystals of intricate morphology are another example of materials design strategies by Nature.[6,7] Although progress is being made in understanding how macromolecules control biomineral formation, the underlying mechanisms responsible for the formation of most biomineralized structures remain elusive.

The key to exploiting the materials construction strategies employed by biomineralizing organisms is to understand what occurs at the interface where biopolymers and inorganic solids coexist.[8] Perhaps the ultimate and most realistic approach would be to analyze the interplay between organic and inorganic components *in situ* within viable biomineralized structures. However, given the complexity within biomineralizing tissues or organisms, the ability to distinguish and map individual events or participants is understandably difficult at the present time. An alternative approach is to utilize defined model biomineralizing systems containing a limited number of molecular participants under controlled conditions. This approach has been used to examine the participation of a number of polypeptides within biomineral nucleation and crystal growth assay systems.[9-17] Although limited in their scope, such *in vitro* systems provide much needed information on the role of proteins within mineralizing systems, and can serve as a stepping stone towards more complex model systems that possess larger numbers of molecular participants.

Our premise is that the involvement of organic macromolecules at mineral interfaces is actually a two-way street: there is interplay between the macromolecular organic components and the mineral, and both are perturbed during the mineralization process. To verify or refute this premise, one needs to analyze molecular features at the organic–mineral interface (OMI). Simple biomineral model systems, composites of only *one* kind of organic molecule and *one*

mineral phase can be quantitatively analyzed, and most importantly the organic and the mineral components of the OMI can be analyzed simultaneously. Here we present a study of the OMI in model biomineralizing systems, wherein we describe the early stages of *in vitro* calcite mineralization under the influence of three mollusk nacre protein-derived sequences (AP7N, AP24N, n16N, each 30 AA, Figure 1)[9,11,13-17] and one protein isolated from sea urchin spicule elements[18-22] (LSM34, 334 AA, Figure 2).

The rationale for selecting the three 30-AA peptides is that these are the binding part of the corresponding proteins AP7, AP24, n16, they affect the morphology of calcite *in vitro*, and do so similarly to the parent proteins, as documented by extensive atomic force microscopy (AFM) and solid state nuclear magneti resonance (NMR) studies.[9,11,13-17]

To examine the molecular features present at the OMI in the organic-mineral systems, we used x-ray absorption near-edge structure (XANES) spectroscopy, a tool sensitive to the electronic and molecular structure. Although XANES cannot provide the complete molecular or mineral three-dimensional structure that diffraction yields, it is exquisitely sensitive to the formation or disruption of chemical bonds, does not require the sample to be crystalline, and can analyze both sides of the OMI in these model systems.

We adopted a building-block approach, in which we first analyzed with XANES spectroscopy each of the polypeptides individually, then pure calcite crystals, and finally calcite crystals grown *in vitro* from solution in the presence of these polypeptides. We find that in

AP7N, AP24N, n16N, and LSM34 polypeptide systems, new spectral features appear in the combined systems, which differ from the two separate components, and from their linear combination. We observe one new peak in XANES spectra, while two other peaks associated with calcite are disrupted by peptide or protein binding. We conclude that at the OMI, calcite CO bonds are affected by polypeptides, while re-arrangements of the peptide or protein conformation leads to more ordered side chains, in better alignment with the polarization of the illuminating soft-x-rays. These effects are less prominent for Asn, Gln-substituted n16NN polypeptide. Collectively, our data suggest that the organic and mineral components do influence one another. The tools and concepts generated by these experiments may ultimately be useful for elucidating authentic biomineralization processes.

MATERIALS AND METHODS

Peptide synthesis and purification. Free amino termini, C-amide-capped peptides were synthesized and purified to mimic their attachment to the protein. The synthesis, purification, and characterization of *Haliotis rufescens*-specific AP7N, AP24N, and *Pictada fucata*-specific n16N mineral modulation domains were performed as described in earlier reports.[9,15-17] A sequence variant of n16N, named n16NN, was also created and purified using the same protocols for n16N.[15] Here, n16NN is the 30 AA n16N sequence where Asp and Glu residues were replaced by Asn and Gln residues, respectively, during solid-phase peptide synthesis. This

peptide variant was created to test whether the replacement of anionic groups with neutral, polar groups of approximately the same van der Waals volume had any impact on polypeptide interaction with calcite.

***In vitro* mineralization with polypeptides**. Calcite growth was done in solutions containing $CaCl_2$, with NH_4CO_3 vapor, and Kevlar (polyimide) fibers to template growth of calcium carbonate crystals[12,13,15,17] in the presence of model peptides. The small but resilient Kevlar threads, are chemically inert. As they are intertwined as in cotton wool but less densely, they provide physical nucleation sites as well as mechanical support for the growth of calcite crystals from the center of a solution, rather than the bottom. This simplifies crystal morphology assessment, and transfer of individual crystals to metal substrates for XANES and X-PEEM analysis. Peptide stock solutions were added to assay containers to create the final peptide assay concentrations of 100 μM peptide. The negative control conditions consisted of no added peptide, and produced simply synthetic calcite. At the conclusion of the assay periods, the assay supernatants were removed via aspiration and the Kevlar fibers were gently washed three times with 3 mL of calcium carbonate-saturated methanol and then dried at 37°C. [12,13,15,17] SEM imaging was conducted using a Hitachi S-3500N SEM microscope at 5 kV after thin Au coating of samples. The SEM images presented in this report are representative of 10-20 different crystals in each assay sample. Cropping of SEM images and adjustment of brightness/darkness and contrast levels were performed using Adobe Photoshop. [12,13,15,17]

LSM34 extraction and purification. LSM34 cDNA[21] was sub-cloned into the Eco-R1 site of the pProEx plasmid vector (Invitrogen). This produces an N-terminal fusion of a His 6 tag to LSM34. The fusion protein was expressed in *E. coli* under the control of a *Lac Z* promoter. After induction with IPTG (isopropylthiogalactoside), the recombinant protein was isolated by binding to a Ni-containing resin according to the directions of the manufacturer (Qiagen). The purified protein was dialyzed against water, precipitated, and dried by lyophilization.

Crystal growth of LSM34-calcite composites. Recombinant LSM34 was dissolved in distilled deionized water (DDW) at concentration 5 mg/ml. The pH of the solution was adjusted to 2.8 with HCl and it was kept for 72 hours at 4ºC. Prior to the mineralization experiments, the solutions were analyzed with dynamic light scattering (DLS), which confirmed that the major fraction of the protein was in a monomeric form. Mineralization was carried out using the ammonium carbonate diffusion process[23] with some modifications. The mineralization reactions were run in 48–well polystyrene plates (Fisher). Glass cover slips were cleaned with a detergent solution in DDH_2O with sonication and rinsed with DDH_2O multiple times to ensure the removal of the surfactant molecules. The glass cover slips were put into separate wells. The wells with coverslips were filled with 1 mL of 10 mM $CaCl_2$ (Sigma). The protein stock solution was added to the well, to a final concentration of 0.2 mg/ml (~6×10^{-6}M). A pinch of $(NH_4)_2CO_3$ powder was placed into a well on the opposite side of the plate and a droplet of water was added to that well. The plate was sealed with Parafilm® and placed into an incubator at 30ºC for 12 hours. The glass slides with calcite crystals were briefly dipped into distilled water and then

rinsed in 2% sodium hypochlorite solution to remove the protein remaining on the surface of the crystals. The cover slips were sequentially dipped in three 0.5 L beakers of DDH_2O and then in 100% ethanol and air-dried.

Geologic calcite. Single crystals of calcite were cut, immersed in trichloroethane in ultrasonic bath for 20 minutes, followed by the same treatment in acetone and then in ethanol. These three cleaning steps are commonly used to eliminate any contaminant or oils from materials before inserting them in ultrahigh vacuum. They were used here to eliminate the peaks previously detected at 285 eV, which is typical of proteins and humic substances. Carbonates are known to absorb such substances from ground water, therefore it was necessary to thoroughly clean geologic calcite before XANES analysis. The peak at 285 eV was completely eliminated by this cleaning procedure.

XANES spectromicroscopy. All samples were analyzed with the Spectromicroscope for PHotoelectron Imaging on Nanostructures with X-rays (SPHINX), which is an X-ray PhotoElectron Emission Microscope (X-PEEM)[24]. The choice to use a spectromicroscope instead of a conventional total electron yield experiment has three advantages. First, a very small amount of material can provide informative data, e.g. single 100-μm calcite crystals. Each crystal is imaged at low magnification (180 μm field of view), stacks of images are acquired while scanning the photon energy across the C and O K-edges, and the Ca L-edge. XANES spectra are then extracted from selected regions of interest on or off the crystal, to provide a simultaneously

acquired background. The second advantage is that the radiation dose can be kept at a minimum, to prevent chemical changes in the analyte due to radiation damage. The radiation dose used for all the data presented here varied between 0.2 and 20 MGy. Doses up to 65 MGy were tested, and spectral changes due to damage were not observed either on calcite crystals or on peptide-crystal composites. Synthetic calcite crystals were tested up to 34 GGy, and damage was observed only above 1 GGy. The third advantage is that the method developed on these simple model biominerals can also be applied to more complex organic-mineral interfaces, as shown in the last figure. Droplets of 500 μM peptide solutions were deposited on Si wafers, air dried, then analyzed with SPHINX with the 1-μL droplet edge in a 180-μm field of view, so a simultaneously acquired background curve could always be extracted from the Si wafer for normalization. The LSM34 protein was analyzed as a powder, pressed into indium foil and coated with 1 nm Pt.[25] Calcite-polypeptide composite crystals were removed from Kevlar threads or glass cover slips using tweezers, then pressed into indium foil and coated with 1 nm Pt[25] for spectromicroscopy analysis. Each XANES spectrum of mineral-organic system reported here was acquired from a single small crystal, and repeated over a minimum of 5 different crystals. The results presented are therefore representative of a larger body of data.

RESULTS

Calcium carbonates are major components of the biomineralized crustacean and mollusk shells, avian eggshells, otoliths, statoliths, coccoliths, as well as the endoskeleton of echinoderms. Their simple lattice structures and controllable mineralization processes *in vitro*

make them interesting model system for examining what occurs at the OMI when polypeptides and proteins are present. Hence, they represent an excellent starting point for examining the interplay between inorganic minerals and polypeptides, such as AP7N, AP24N, and n16N, which modulate the growth and morphology of calcite crystals *in vitro* (Figure 3).[11,14-16]

In Supporting Figure S1-S4 we report lower magnification scanning electron microscopy (SEM) images of these samples, to show that the majority of crystals have similar morphologies, thus the ones analyzed by XANES spectroscopy in X-PEEM are representative.

Interestingly, AP7N and AP24N, which exhibit unfolded, conformationally labile structures in solution, generate very similar blocking effects on calcite crystal growth, but are kinetically different, with AP24N exhibiting enhanced activity over AP7N.[9,11] On the other hand, n16N affects calcium carbonate growth and morphology in a manner that is strikingly different from either AP7N or AP24N,[11,15,17] and assembles into beta-strand dimers under *in vitro* mineralization conditions.[15] Hence, these sequences can provide us with comparative data regarding polypeptide – mineral associations and structure.

In Figure 4 we present total electron yield (TEY) and fluorescence yield (FY) spectra of geologic calcite, and TEY of synthetic calcite. Fluorescence yield is bulk-sensitive, while TEY is only sensitive to the surface (3 nm at the carbon edge). The two TEY spectra from geologic and synthetic calcite are very similar, ruling out the possibility that the spectral variations reported below are due to synthetic calcite growth conditions or contamination. FY was done to confirm that all peaks observed in the TEY spectrum of geologic and synthetic calcite are indeed due to

the calcite structure and not to its surface states or contamination. The results are further validated by peak fitting, as reported in Supporting Figure S5 and Table S1. The main peaks present in calcite XANES spectra are those due to the C1s→π* of the C=O double bond, and the C1s→σ* of the C–O single bond and of the C=O double bond. These two peaks, at 290.3 eV and 301.5 eV, respectively, are expected from the crystal structure and the chemical bonds present in bulk calcite, and are present in calcite, aragonite and dolomite. Other less intense peaks at 295 eV and 298 eV are present both in aragonite and calcite. These are also associated with the CO bonds and are part of a rich C1s→σ* manifold. Their polarization dependence coincides with that of the main σ* peak at 301.5 eV.[28] The other calcite peak at 288 eV is not polarization dependent, and it's origin is unknown. We note that this peak is absent from the FY bulk spectrum, suggesting that this is a surface state. Although peaks at this energy in proteins and peptides are assigned to C=O in the peptide bond, in pure, clean calcite such peak was not expected. This peak cannot be due to surface contamination, as in the synthetic calcite there were no proteins or peptides in solution, and in geologic calcite all traces of protein were removed by thorough cleaning, as shown by the disappearance of the peak at 285 eV. The peak at 288 eV is therefore likely due to calcite surface reconstruction or termination. Furthermore, the similarity of geologic calcite and negative control synthetic calcite rules out the possibility that the peak intensity variations observed below are due to adsorption of contaminants during synthetic crystal growth, and can only be due to OMI effects.

In comparison with calcite alone, the XANES spectrum for calcite crystals grown *in vitro*

on Kevlar threads in the presence of AP7N, AP24N, and n16N is dramatically affected (Figures 5, 6, and 7). The peptide spectra exhibit the well-known π* peak at 285 eV, due to the C=C double bonds present in the His, Phe, Trp and Tyr residues (H, F, W, Y, highlighted in cyan in the sequences shown in Figure 1). They also all exhibit the π* peak at 288 eV, due to the C=O double bond present in all peptide bonds, [29] as well as the carboxyl groups of Asp and Glu side chains. The peak at 289 eV, present with varying intensities in all spectra is assigned to the C=N π* resonance, present only in Arg (R).[30]

XANES spectra obtained for the peptide-calcite crystals exhibit distinct differences, compared with the two spectra of the separate components. Notice in particular that two peaks at 295 eV and 298 eV are prominent in calcite but are disrupted in AP24N-modulated calcite. Another peak at 287 eV, not originally present in either AP24N or in calcite, appears in AP24N-modulated calcite. All three peaks arise from C1s→σ* transitions, and are less studied in the field of carbon XANES spectroscopy. The peak at 287 eV is well known to correspond to C-H single bond,[30-32] while the other two σ* peaks in calcite are due to CO bonds.

The peptides AP7N and n16N produce effects very similar to AP24N (Figures 5 and 6). Specifically, the peaks at 295 eV and 298 eV are decreased in intensity, while the peak at 287 eV is much enhanced. The negatively charged Asp and Glu amino acids are expected to form bonds with hydrated Ca ions in solution and at calcite step edges.[33,34] Interestingly, these effects are greatly reduced for crystals grown in the presence of Asn, Gln – substituted n16NN (Figure 7).

Specifically, n16N dramatically suppresses the peaks at 295 and 298 eV and enhances the one at 287 eV while n16NN has a much smaller effect. Note that the AP7N – calcite sample exhibits a greater degree of spectral noise relative to the AP24N – calcite sample; this is the result of the higher binding affinity that AP24N exhibits for calcium carbonates compared to AP7N.[9]

To compare our nacre polypeptides with another polypeptide, derived from a calcite-based tissue that is not molluscan in origin, we extended the XANES spectroscopy study to include a native protein isolated from the sea urchin spicule matrix, LSM34. As shown in Figure 8, the results obtained from calcium carbonate crystals grown in the presence of LSM34 are consistent with the findings of the nacre systems. Specifically, the LSM34 protein decreased the intensity of the calcite peaks at 295 eV and 298 eV, but significantly broadened the peak centered at 288 eV, thus including the peak at 287 eV. Surprisingly, the effects that LSM34 and the nacre polypeptides have on specific bonds in *in vitro*-synthesized calcite are similar, demonstrating that there are general phenomena occurring at the OMI in these different systems. It remains to be seen whether these phenomena can also be observed *in situ* at OMI regions within molluscan nacre and sea urchin calcitic spicules.

To quantify spectral peak variations, we fit all spectra with 11 Gaussians and 1 arctangent. The complete results of peak fitting for all spectra presented here are reported graphically in Supporting Figure S6 and numerically in Supporting Table S2. In summary, the most significant changes introduced by organic-mineral interaction concern the intensities of

three peaks labelled peaks 2, 7 and 9, at energies 287 eV, 295 eV, and 298 eV, respectively, corresponding to C-H bonds in peptides, and CO bonds in calcite. These peak variation was already visible in the raw spectra. Furthermore, peak fitting revealed another significant change that was more difficult ot appreciate in the raw data: the broad peak 6 at ~294 eV increases upon mineral binding of AP24N, AP7N and n16N. The assignment of this peak is unclear at present. As this peak is not present either in calcite or in peptides alone, it must originate from the peptide-mineral interface. We tentatively assign it the C-O σ^* in carboxylate groups, which we previously observed at the same energy in a different organic-biomineral system (acidic polysaccharide-FeOOH)[38] which was enhanced only upon mineral binding of the carboxyl groups. Figure 9 shows these results synthetically in a histogram, while Supporting Table S2 shows the complete set of fit parameters for all samples.

Furthermore, peak fitting of the TEY and FY spectra of geologic calcite, presented in Figure S5 and Table S1, demonstrate that all peaks observed in the surface sensitive TEY spectrum are also present in the bulk sensitive FY spectrum, and are therefore associated with the bulk calcite crystal structure, not with its surface.

DISCUSSION

The importance of σ* peaks is rarely discussed in carbon XANES spectroscopy. This is due in part to the inconspicuous appearance of these peaks, often too broad or not sufficiently intense to be spectroscopically distinct. The CO and C–H single bonds that give rise to these spectral features, however, are the most abundant in organic polymers, and therefore extraordinarily relevant. This work demonstrates that upon mineral binding the C–H peak is enhanced by three peptides and one protein, AP24N, AP7N, n16N and LSM34. Since the C–H species is located at conformationally sensitive regions of polypeptides (i.e., side chain C–H), we propose that the prominence of this peak is due to ordering of the amino acid side chains as a consequence of polypeptide association with the mineral phase. This is an interesting finding, given that the solution structures of AP7N, AP24N, and n16N are largely unfolded and exhibit conformational lability,[9,13-17] and it suggests that conformational reordering is occurring in these sequences once they become affiliated with calcium carbonates. A similar enhancement of the C–H single bond peak was obtained by the Ade group in an abiotic system: ethylene-1-alkene copolymers, differing only in length and frequency of polymer branches. Because of the chemical simplicity of that system, C-H peak enhancement must be due to either or both the degree of conformational ordering, or the intermolecular interactions between polymer branches.[31] The presence of polypeptide reordering is very similar to that obtained by our group on amyloid forming peptides. In that case as well, upon amyloid fibril formation, the C–H bond is enhanced, due to ordering of the amino acid side chains.[32] Thus, some degree of polypeptide ordering also

occurs when polypeptide – mineral composites are formed, as presented here. Increased ordering in polypeptide chains upon mineral binding has been previously observed for statherin, another biomineral protein, which is present in the saliva solution as a random coil, and becomes alpha helical after binding to the hydroxyapatite teeth mineral. [35-37]

Interestingly, the other main result we obtained, the disruption of peaks at 295 eV and 298 eV, also highlights the importance of σ* peaks in biominerals. These two σ* peaks, due to CO bonds in calcite, are reminiscent of the peak observed in a natural biomineral system, composed of FeOOH nanoparticles and bacterially produced polysaccharides bound to each other, [38] where we hypothesized a templating mechanism, with binding of carboxyl groups in polysaccharides to Fe atoms in FeOOH nanoparticles. The σ* peak observed upon biomineral formation in that case was a C–O single bond at 292.4 eV.[38] The σ* peaks, originating from C–H, C–O, C=O or other bonds, are observed at 287 eV or above 291 eV. This spectral region is often featureless in carbon XANES spectra of biopolymers. The heterogeneity of bond angles, combined with the rotational freedom around single bonds makes these σ* peaks either too broad or not sufficiently intense to be resolved. Upon mineral binding, however, the degrees of freedom that polymers had in solution are greatly decreased, and correspondingly the molecular configurations become more rigid, homogeneous, and aligned with each other: in one word, more *ordered*. Under the linearly polarized x-ray illumination[#], increased molecular order generates more intense, narrower, and therefore spectroscopically distinct σ* peaks. This interpretation of

[#] Synchrotron radiation is always linearly polarized in the orbit plane, that is, horizontally.

the results observed here on C–H, and previously on C–O[38] is tentative. If and when other techniques yield the structure of these peptides in the presence of calcium carbonates, we will be able to substantiate this interpretation of the current results.

Another main result of this study is the appearance of a new peak upon mineral binding. This peak at ~294 eV is tentatively assigned to C-O σ* in mineral-bound carboxylate groups, and is reminiscent of a peak previously found at 294.2 eV to appear upon organic-mineral bond formation in acidic polysaccharides templating the formation of pseudo-single crystals of akaganeite at the core of ferrihydrite nanoparticle filaments in bacterial biofilms.[38] In the present systems the peak is much broader, possibly due to greater etherogeneity of the peptide-calcite carboxylate bonds compared to the carboxylate-akaganeite bonds. Comparison of n16N and n16NN (e.g. supporting Figure S6), with and without Asp and Glu, respectively, supports the association of peak 6 at 294 eV with carboxylate groups, as this peak is very intense in calcite grown in the presence of n16N and completely absent from n16NN.

Furthermore, the Asn, Gln-modified n16NN peptide does not appear to have substantial interactions with calcium carbonates, as evidenced by the minimal CO bonds disruption in calcite (Figure 7) and the absence of C-H peak enhancement. Thus, it seems likely that CO bond disruption arises in response to interactions of the mineral phase with anionic side chains. Similarly, the enhancement of the C–H peak probably occurs as a result of Asp and Glu interactions at the mineral interface. Thus, the involvement of anionic amino acids in

polypeptide – mineral binding is an important part of the OMI region and a likely contributor to conformational ordering of these polypeptides on mineral interfaces. Ordering of homopolypeptides upon mineral binding was previously reported by the Dove-De Yoreo group. In that study aspartic acid formed an ordered adsorption layer on calcite surfaces.[39] Additional investigations are currently underway to assess the importance of Asp and Glu residues in n16N, AP7N, and AP24N.

One point still unresolved is the localization of polypeptide species on or within (i.e., occluded) *in vitro* synthesized calcium carbonates. It is not known at present whether or not the nacre polypeptides AP7N, AP24N, and n16N are localized exclusively at exposed interfaces of crystals, or if they also become occluded within the crystals during the mineral formation process *in vitro*. Interestingly, AFM imaging studies of calcite hillock growth in the presence of AP7N and AP24N demonstrate the formation of amorphous-appearing deposits on exposed terrace surfaces, which eventually become incorporated as part of the growth front.[11] If we presume that these peptides exist as polypeptide-mineral complexes within these deposits, then it is likely that the peptides may eventually become sub-surface species as the crystal grows and incorporates these deposits. In the case of the spicule matrix protein, LSM34, it is known that this protein becomes occluded within spicule calcite crystals, and we speculate that this process also occurs *in vitro*. However, since XANES spectromicroscopy is a surface sensitive technique (probing a maximum depth of 3 nm from the surface[40]), the CO bond disruption observed in the peptide-mineral systems might only be at the surface of the crystals. Therefore, we could not

determine if the protein and peptides are only surface bound or also occluded, bonded or trapped inside composite crystals. Thus, verification of occluded polypeptide species requires additional study, and this is currently in progress.

As evidenced by enhancement of the polypeptide-associated C–H peak, there appears to be ordering or rearrangement of polypeptide structure in our *in vitro* model polypeptide – mineral systems.

Cölfen and Mann proposed a cooperative relationship between assembling organic molecules and forming crystals, in which these two components dynamically influence each other.[41] Beniash et al. also proposed this mechanism for dental enamel.[42] The present results from XANES spectromicroscopy of simple biomineral model systems appear to confirm the hypothesis that there is interplay between polypeptides and the mineral phase.

These results are the first of a systematic study we have initiated and that we plan to pursue extensively. The ultimate goal is the understanding of the OMI in natural biominerals, such as sea urchin spicules, spines and nacre, and how templating and self-assembly of crystals are directed and controlled by the organic molecules in these complex biominerals. Spectromicroscopy of nacre is possible today, as shown in Figure 10, but the interpretation of the spectroscopic results is at present impossible, due to the many components involved. We intend to build, block by block, a system of organic-mineral interactions that are spectroscopically distinguishable, and that have the potential to elucidate the fundamental

mechanisms associated with biomineral formation. The present work is a modest first step.

ACKNOWLEDGEMENTS

We are grateful to Ben Gilbert for writing the Igor® Procedures for C spectra normalization. This work was supported by NSF awards PHY-0646018 and CHE-0613972, DoE Award DE-FG02-07ER15899, UW-Graduate School Romnes and Vilas Awards to PUPAG. The experiments were performed at the UW-SRC, supported by NSF award DMR-0537588. Portions of this work were supported by funding from the Department of Energy (DE-FG02-03ER46099, to JSE) and represent Contribution 36 from the Laboratory for Chemical Physics, New York University.

SUPPORTING INFORMATION. Supporting Information includes 6 figures (4 SEM micrographs and 2 peak-fitted sets of spectra) and 2 tables presenting the results of peak fitting for all spectra presented here.

REFERENCES (to be shortened after the reviewing process)

1. Mann S., Biomineralization: Principles and Concepts in Bioinorganic Materials Chemistry, *Oxford Univ. Press*, Oxford, **2001**.
2. Biomineralization, Vol. 54, Eds. PM Dove, JJ De Yoreo, S Weiner, *Mineralogical Society*

of America, **2004**, Washington DC, p. 57-93.

3. Lowenstam, H.A.; Weiner, S. On Biomineralization. Oxford University Press, Oxford, **1989**.
4. Grotzinger, J.P. Waters, W.A. Knoll, A.H. Paleobiology **2000**, 26, 334.
5. Currey, J., D. Mechanical properties of mother of pearl in tension. *Proc R Soc Lond B* **1977**, 196, 443.
6. Wilt, F. H. Matrix and Mineral in the Sea Urchin Larval Skeleton. *J. Struct. Biol.* **1999**, 126, 216–226.
7. Meldrum, F. C. Calcium carbonate in biomineralisation and biomimetic chemistry. *Int. Mater. Rev.* **2003**, 48, 187-224.
8. PUPA Gilbert, BH Frazer and M Abrecht. The organic-mineral interface in biominerals. Reviews in Mineralogy and Geochemistry. In: Molecular Geomicrobiology. Vol 59. JF Banfield, KH Nealson, J. Cervini-Silva (eds), *Mineralogical Society of America*, Washington DC, p 157-185, **2005**.
9. Collino, S, Evans, JS, (2007) Molecular characterization of a mineral modification subdomain of the aragonite associated protein, AP24. Biomacromolecules, in press.
10. Kulp, JL III, Minamisawa, T, Shiba, K, Evans, JS (2007) Conformational properties of an artificial protein that regulates the nucleation of inorganic and organic crystals. Langmuir 23: 3857-3863.
11. Kim, IW, Darragh, MR, Orme, C, Evans, JS (2006) Molecular "tuning" of crystal growth by nacre-associated polypeptides. Crystal Growth and Design, 5: 5-10.

12. Collino, S, Kim, IW, Evans, JS, (2006) Identification of an “acidic” C-terminal mineral modification sequence from the mollusk shell protein, Asprich. Crystal Growth and Design, 6: 839-842.

13. Kim, IW, Collino, S, Morse, DE, Evans, JS (2006) A crystal modulating protein from molluscan nacre that limits the growth of calcite *in vitro*. Crystal Growth and Design, 6: 1078-1082.

14. Kim, IW, Morse, DE, Evans, JS (2004) Molecular characterization of the 30-AA N-terminal mineral interaction domain of the biomineralization protein AP7. Langmuir 20: 11664-11673.

15. Kim, IW, DiMasi, E, Evans, JS, (2004) Identification of mineral modulation sequences within the nacre-associated oyster shell protein, n16. Crystal Growth and Design 4: 1113 – 1118.

16. Wustman, BA, Morse, DE, Evans, JS (2004) Structural characterization of the N-terminal mineral modification domains from the molluscan crystal-modulating biomineralization proteins, AP7 and AP24. Biopolymers 74: 363-376.

17. Michenfelder, M, Fu, G, Lawrence, C, Weaver, JC, Wustman, BA, Taranto, L, Evans, JS (2003) Characterization of two molluscan crystal-modulating biomineralization proteins and identification of putative mineral binding domains. Biopolymers 70: 522-533; errata 73: 299.

18. Benson, S., Sucov, L, Stephens, L, Davidson, E.H. & Wilt, F.H. Lineage specific gene encoding a matrix protein of the sea urchin embryo spicule. I. Authentication of the

cloned gene and its expression. *Dev. Biol.* **1987**, 120, 499-506.

19. Sucov, H., Benson, S., Robinson, J. Wilt, F. and Davidson, E. Lineage specific gene encoding a major matrix protein of the sea urchin embryo spicule. II. Structure of the gene and derived sequence of the spicule matrix protein. *Dev. Biol.* **1987**, 120, 507-519.
20. Katoh-Fukui, YK., Noce, T., Ueda, T. Fujiwara, Y, Hashimoto, N, Higashinakagawa, T., Killian, C.E., Livingston, B.T., Wilt, F.H., Benson, S.C., Sucov, H.M., and Davidson, E.H. The corrected structure of the SM50 spicule matrix protein of Strongylocentrotus purpuratus. *Dev. Biol.* **1991**, 145, 201-202.
21. Livingston, B.T. Shaw, R., Bailey, A. and Wilt. F. Characterization of a cDNA encoding a protein involved in formation of the skeleton during development of the sea urchin, *Lytechinus pictus*. *Dev. Biol.* **1991**, 148, 473-480.
22. Peled-Kamar, M., Hamilton, P., and Wilt, F.H. The Spicule Matrix protein LSM34 is essential for biomineralization of the sea urchin spicule. *Exp. Cell Res.* **2002**, 272, 56-61.
23. Albeck, S., Aizenberg, J., Addadi, L., Weiner, S. Interactions of various skeletal intracrystalline with calcite crystals. J. Am. Chem. Soc. **1993**,115, 11691-11697.
24. Frazer BH, Girasole M, Wiese LM, Franz T, De Stasio G. Spectromicroscope for the PHotoelectron Imaging of Nanostructures with X-rays (SPHINX): performance in biology, medicine and geology. *Ultramicroscopy* **2004**, 99, 87-94.
25. G De Stasio, BH Frazer, B Gilbert, KL Richter and JW Valley, Compensation of charging in X-PEEM: a successful test on mineral inclusions in 4.4 Ga old zircon. *Ultramicroscopy* **2003**, 98, 57-62.

26. Graf, D.L., *Amer. Mineral.* **1961**, 46, 1283-1316.

27. Myneni, S.C.B. Reviews in Mineralogy and Geochemistry, Applications of Synchrotron Radiation in Low Temperature Geochemistry and Environmental Science. Fenter, P.A., Rivers, M.L., Sturchio, N.C., Sutton, S.R. Eds. *Mineralogical Society of America*, Washington, DC, **2002**, 49, 485-571.

28. Metzler, R.A., Abrecht, M., Olabisi, R.M., Ariosa, D., Johnson, C.J., Frazer, B.H., Coppersmith, S.N., Gilbert, P.U.P.A. Columnar Nacre Architecture and Possible Formation Mechanism. *Phys. Rev. Lett.* **2007** 98, 268102-1/4. Also featured in *Science* **2007** 317, 175.

29. Gordon, M.L., Cooper, G., Morin, C., Araki, T., Turci, C.C., Kaznatcheev, K., Hitchcock, A. P. Inner-shell excitation spectroscopy of the peptide bond: comparison of the C1s, N1s and O1s spectra of glycine, glycyl-glycine, and glycyl-glycyl-glycine. *J. Phy. Chem. A* **2003** 107, 6144-6159.

30. K. Kaznacheyev, A. Osanna, C. Jacobsen, O. Plashkevych, O. Vahtras, H. Ågren, V. Carravetta, A. P. Hitchcock. Innershell Absorption Spectroscopy of Amino Acids. *J. Phys. Chem. A* **2002**, 106, 3153-3168.

31. Scholl, A., R. Fink, E. Umbach, G.E. Mitchell, S.G. Urquhart and H. Ade. Towards a detailed understanding of the NEXAFS spectra of bulk polyethylene copolymers and related alkanes. *Chem. Phys. Lett.* **2003**, 370, 834-841.

32. CJ Johnson, RM Olabisi, RA Metzler, B Gilbert, BH Frazer, MK Gilles, T Tyliszczak, JA Pedersen, D McKenzie, JM Aiken, and PUPA Gilbert. X-ray spectromicroscopy

captures cross-b fibril structure. *J. Am. Chem. Soc.* **2007**, under review.

33. SR Qiu, A Wierzbicki, EA Salter, S Zepeda, CA Orme, JR Hoyer, GH Nancollas, AM Cody, JJ De Yoreo. Modulation of Calcium Oxalate Monohydrate Crystallization by Citrate through Selective Binding to Atomic Steps. *J. Am. Chem. Soc.* **2005**, 127, 9036-9044.
34. S. Elhadj, E. A. Salter, A. Wierzbicki, J. J. De Yoreo, N. Han, and P. M. Dove. Peptide Controls on Calcite Mineralization: Polyaspartate Chain Length Affects Growth Kinetics and Acts as a Stereochemical Switch on Morphology. *Cryst. Growth & Des.* **2006**, 6, 197-201.
35. PS Stayton, GP Drobny, WJ Shaw, JR Long, M Gilbert. Molecular recognition at the protein-hydroxyapatite interface. *Crit. Rev. Oral Biol. Med.* **2003**, 14, 370-376.
36. JR Long, WJ Shaw, PS Stayton, GP Drobny. Structure and dynamics of hydrated statherin on hydroxyapatite as determined by solid-state NMR. *Biochemistry* **2001**, 40, 15451-5.
37. Shaw, W. J.; Long, J. R.; Campbell, A. A.; Stayton, P. S.; Drobny, G. P. A Solid State NMR Study of Dynamics in a Hydrated Salivary Peptide Adsorbed to Hydroxyapatite. *J. Am. Chem. Soc.* **2000**, 122, 7118-7119.
38. Chan CS*, De Stasio G*, Welch SA, Girasole M, Frazer BH, Nesterova MV, Fakra S, Banfield JF. *equal contributors. Microbial polysaccharides template assembly of nanocrystal fibers. *Science* **2004**, 303, 1656-8.
39. Teng, H.H., Dove, P.M., Orme, C.A., De Yoreo. Baseline for understanding biomineral

formation, *Science* **1998**, 282, 724-727.

40. Frazer, B.H., Gilbert, B., Sonderegger, B.R., De Stasio, G. The probing depth of total electron yield in the sub keV range: TEY-XAS and X-PEEM, *Surface Science* **2003**, 537, 161-167.
41. Cölfen, H., and Mann, S. Higher-Order Organization by Mesoscale Self-Assembly and Transformation of Hybrid Nanostructures. *Angew. Chem. Int. Ed.* **2003**, 42, 2350-2365.
42. Beniash, E., Simmer, J.P., Margolis, H.S. The effect of recombinant mouse amelogenins on the formation and organization of hydroxyapatite crystals *in vitro*. *J. Struct. Biol.* **2005**, 149, 182–190.

FIGURE LEGENDS

Figure 1. Primary sequences of nacre-associated polypeptides. AP7N represents the 30 AA mineral modulating N-terminal domain of the AP7 protein; AP24N AP7N represents the 30 AA mineral modulating N-terminal domain of the AP24 protein. Both AP7 and AP24 are localized in the nacre layer of the Pacific Red abalone, *Haliotis Rufescens*. N16N represents the 30 AA mineral modulating N-terminal domain of the n16 protein, which is located within the nacre pearl of the Japanese oyster, *Pictada fucata*. The n16NN polypeptide is merely the n16N sequence, with Asn substituting for Asp and Gln substituting for Gln. The negatively charged Asp and

Glu amino acids (D and E) are highlighted in yellow, while their positively charged analogues Asn and Gln (N and Q) are highlighted in green. For clarity in discussions below, the amino acids with a C=C double bond are highlighted in cyan. These are His, Phe, Trp and Tyr (H, F, W, Y). The only amino acid with a C=N double bond, Arg (R), is highlighted in magenta.

Figure 2. Primary sequence of LSM34. This protein also contains Asp and Glu (17 residues, highlighted in yellow), as well as Arg (18 residues, highlighted in magenta).

Figure 3: SEM images of calcium carbonate crystal grown on Kevlar threads in the presence of: (A) negative control (no peptide added); (B) AP24N; (C) AP7N; (D) n16N. Assay peptide concentrations were all 100 μM. Notice the dramatic morphological changes introduced by the peptides in the growth solution. Scale bar = 10 μm. Lower magnification SEM images of the same samples are presented in supporting Figure S1-S4.

Figure 4: Comparison of XANES spectra acquired in total electron yield (TEY) and fluorescence yield (FY) on geologic calcite, and negative control synthetic calcite as in Figure 3A. TEY is surface-sensitive while FY is bulk-sensitive. All peaks present in both spectra are associated with the bulk crystal structure of calcite. Notice the similarity of all relevant peaks labeled "π* C=O carbonates" and "σ* CO carbonates". The only peak dissimilar in surface and bulk calcite is at 288 eV, and this peak is likely due to surface reconstruction or termination.

Figure 5: Comparison of XANES spectra acquired with SPHINX on geologic calcite, AP24N polypeptide, and calcite crystals grown on Kevlar threads in the presence of 100 μM AP24N in solution, then separated from it. These crystals represent a composite of calcite + AP24N, and this is spectroscopically distinct from calcite and AP24N alone. Peaks of interest are indicated by cyan vertical lines. The presence and intensity of the 301.5 eV σ* peak indicates that the suppression of the 295 eV and 298 eV peaks is not a polarization dependent effect since the polarization dependence of all three peaks are correlated. This observation is true for all systems examined.

Figure 6. Comparison of XANES spectra acquired with SPHINX on geologic calcite, AP7N polypeptide, and a calcite crystal separated from a Kevlar thread on which it was grown, in the presence of 100 μM AP7N in solution. The latter exhibits the same differences seen in Figure 5, with the differing peaks indicated by cyan lines.

Figure 7. Comparison of XANES spectra acquired with SPHINX on geologic calcite, n16N and n16NN polypeptides, and a calcite crystal grown on a Kevlar thread in the presence of 100 μM n16N or n16NN in solution.

Figure 8. XANES spectra of the LSM34 sea urchin spicule protein, geologic calcite, and calcite crystals grown in the presence of LSM34 in solution. The LSM34 spectrum exhibits an unusually intense π* peak at 289.4 eV, which corresponds to the C=N double bond, only

present in Arg (R). The Arg residues in the sequence of this protein justify the presence of this peak, although it's intensity, greater than the carboxyl C=O, is surprising. The effect of LSM34 on calcite is similar to that observed in Figures 5, 6, 7 and is also highlighted by cyan lines.

Figure 9. Variation of the peak areas for the three peaks that vary the most upon organic-mineral binding, in all analyzed systems. Complete plots and detailed peak-fitting parameters are provided in the supporting Figure S6 and Table S2.

Figure 10. SPHINX image (yellow tritone) and Ca and C distribution maps (magenta and blue tritones) acquired on the polished surface of a cross-section of nacre from red abalone. The nacre layers are interrupted by a crack that the animal healed during its life. The nacre surface and mantle cells were at the bottom right of this field of view, parallel to the nacre layers. Notice the different orientation of the nacre layers in the healed crack compared to the surrounding nacre tissue, and the much larger concentration of carbon (white = high concentration) around the crack edges, which are Ca-poor.

FIGURES

AP24N: ADDDEDASSGLCNQYNQNVTTRPNNKPKMF

AP7N: DDNGNYGNGMASVRTQGNTYDDLASLISYL

n16N: AYHKKCGRYSYCWIPYDIERDRYDNGDKKC

n16NN: AYHKKCGRYSYCWIPYNIQRNRYNNGNKKC

Figure 1. Primary sequences of nacre-associated polypeptides. AP7N represents the 30 AA mineral modulating N-terminal domain of the AP7 protein; AP24N AP7N represents the 30 AA mineral modulating N-terminal domain of the AP24 protein. Both AP7 and AP24 are localized in the nacre layer of the Pacific Red abalone, *Haliotis Rufescens*. N16N represents the 30 AA mineral modulating N-terminal domain of the n16 protein, which is located within the nacre pearl of the Japanese oyster, *Pictada fucata*. The n16NN polypeptide is merely the n16N sequence, with Asn substituting for Asp and Gln substituting for Gln. The negatively charged Asp and Glu amino acids (D and E) are highlighted in yellow, while their positively charged analogues Asn and Gln (N and Q) are highlighted in green. For clarity in discussions below, the amino acids with a C=C double bond are highlighted in cyan. These are His, Phe, Trp and Tyr (H, F, W, Y). The only amino acid with a C=N double bond, Arg (R), is highlighted in magenta.

MKGLLLILASLVAIATGQDCPAYYVRSSSGASCYRYFNIRVLHRMASEFCEMVTP
CGNGPSRMGALASISSPIENHEVYRMVASFSQDNQMENEAWLGWNTQSPRFWE
DGTPAYPNGFAGFHQSGSYTSWPSWRPGMPTSGWPVNPANPWTPPPGRAPVMK
GQHVTPQQPGQRPNLGPEWDVEATAMRAFVCEVAAGQNIPPGQQPGFGGQQPG
FGGRQPGFGGQQPGFGQQPGFGGRQPGFGGRQPGFGGQQPGFGGQQPGFGGQQ
PGFGGQQPGFGGQQPGFGGQQPGFGGQQPGFGGGPQRPGMGGQPNSPNPRFNR
PRMLQEAETDVTGS

Figure 2. Primary sequence of LSM34. This protein also contains Asp and Glu (17 residues, highlighted in yellow), as well as Arg (18 residues, highlighted in magenta).

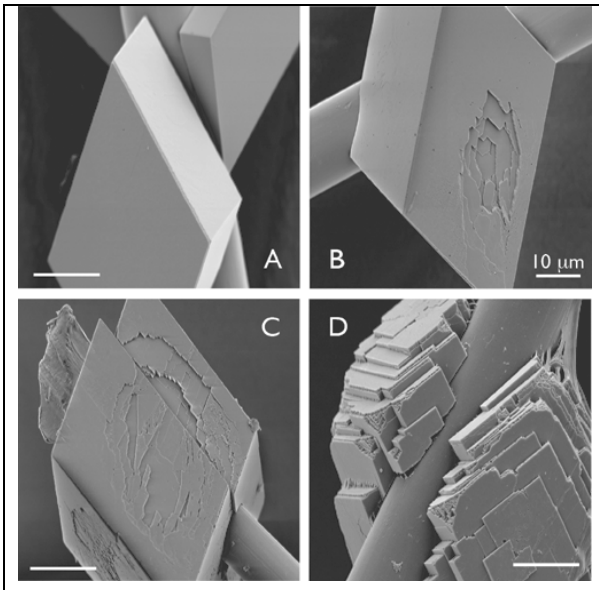

Figure 3: SEM images of calcium carbonate crystal grown on Kevlar threads in the presence of: (A) negative control (no peptide added); (B) AP24N; (C) AP7N; (D) n16N. Assay peptide concentrations were all 100 µM. Notice the dramatic morphological changes introduced by the peptides in the growth solution. Scale bar = 10 µm. Lower magnification SEM images of the same samples are presented in supporting Figure S1-S4.

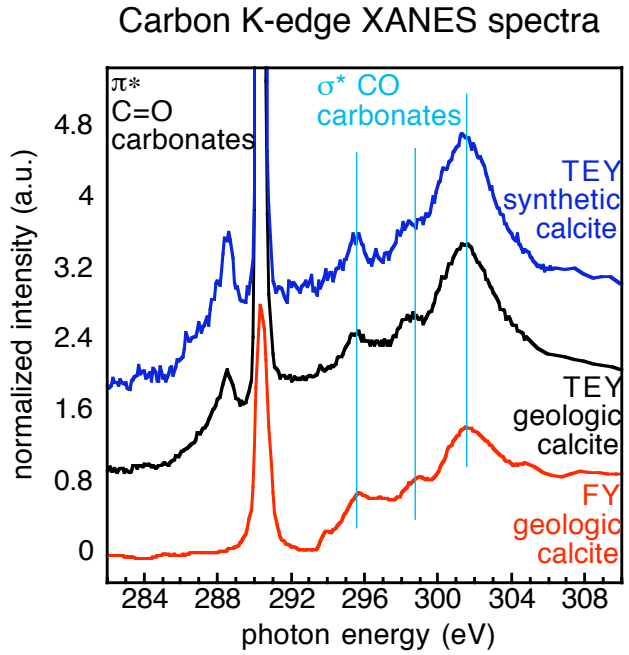

Figure 4: Comparison of XANES spectra acquired in total electron yield (TEY) and fluorescence yield (FY) on geologic calcite, and negative control synthetic calcite as in Figure 3A. TEY is surface-sensitive while FY is bulk-sensitive. All peaks present in both spectra are associated with the bulk crystal structure of calcite. Notice the similarity of all relevant peaks labeled "π* C=O carbonates" and "σ* CO carbonates". The only peak dissimilar in surface and bulk calcite is at 288 eV, and this peak is likely due to surface reconstruction or termination.

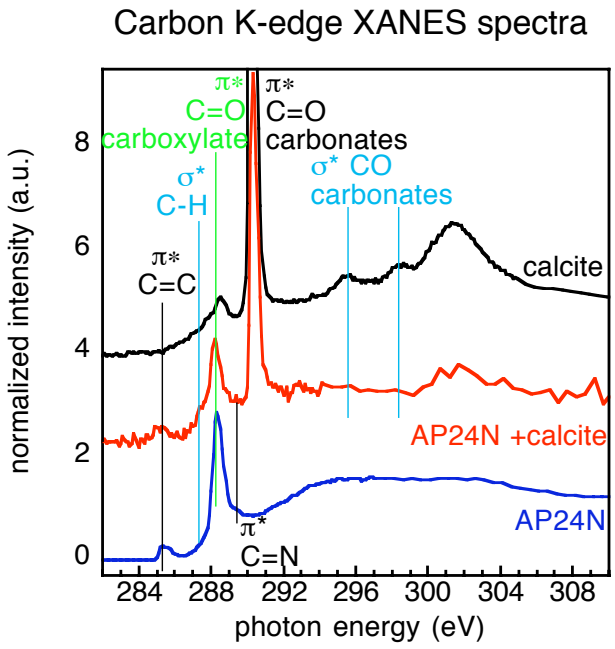

Figure 5: Comparison of XANES spectra acquired with SPHINX on geologic calcite, AP24N polypeptide, and calcite crystals grown on Kevlar threads in the presence of 100 µM AP24N in solution, then separated from it. These crystals represent a composite of calcite + AP24N, and this is spectroscopically distinct from calcite and AP24N alone. Peaks of interest are indicated by cyan vertical lines. The presence and intensity of the 301.5 eV σ* peak indicates that the suppression of the 295 eV and 298 eV peaks is not a polarization dependent effect since the polarization dependence of all three peaks are correlated. This observation is true for all systems examined.

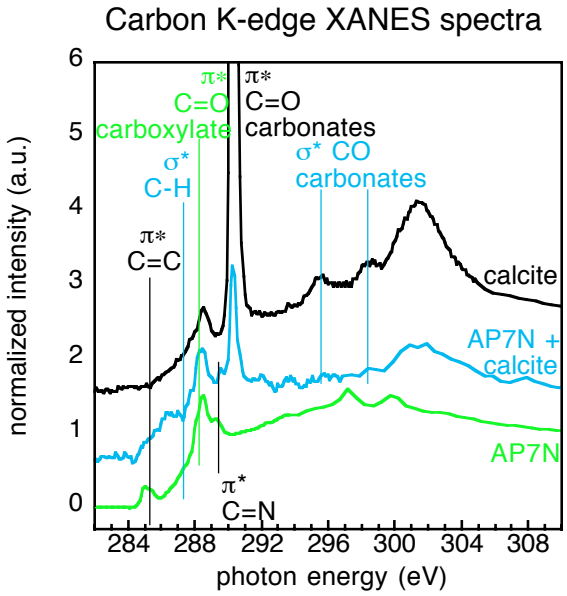

Figure 6. Comparison of XANES spectra acquired with SPHINX on geologic calcite, AP7N polypeptide, and a calcite crystal separated from a Kevlar thread on which it was grown, in the presence of 100 µM AP7N in solution. The latter exhibits the same differences seen in Figure 5, with the differing peaks indicated by cyan lines.

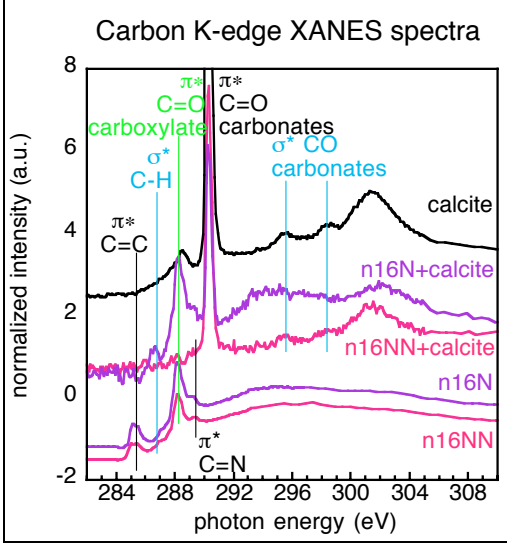

Figure 7. Comparison of XANES spectra acquired with SPHINX on geologic calcite, n16N and n16NN polypeptides, and a calcite crystal grown on a Kevlar thread in the presence of 100 μM n16N or n16NN in solution.

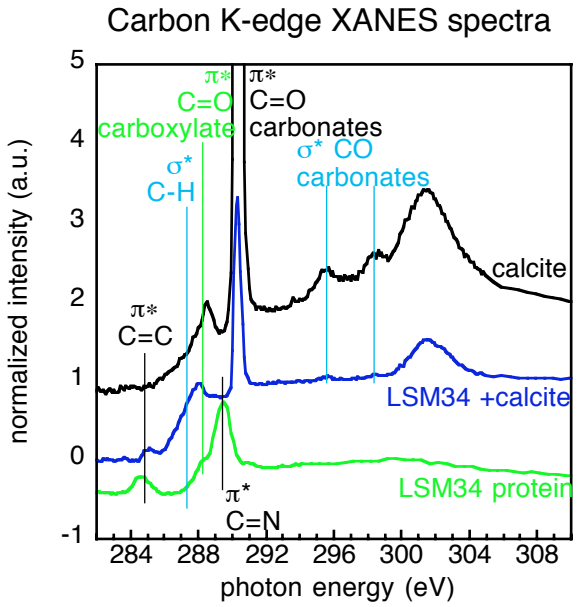

Figure 8. XANES spectra of the LSM34 sea urchin spicule protein, geologic calcite, and calcite crystals grown in the presence of LSM34 in solution. The LSM34 spectrum exhibits an unusually intense π* peak at 289.4 eV, which corresponds to the C=N double bond, only present in Arg (R). The Arg residues in the sequence of this protein justify the presence of this peak, although it's intensity, greater than the carboxyl C=O, is surprising. The effect of LSM34 on calcite is similar to that observed in Figures 5, 6, 7 and is also highlighted by cyan lines.

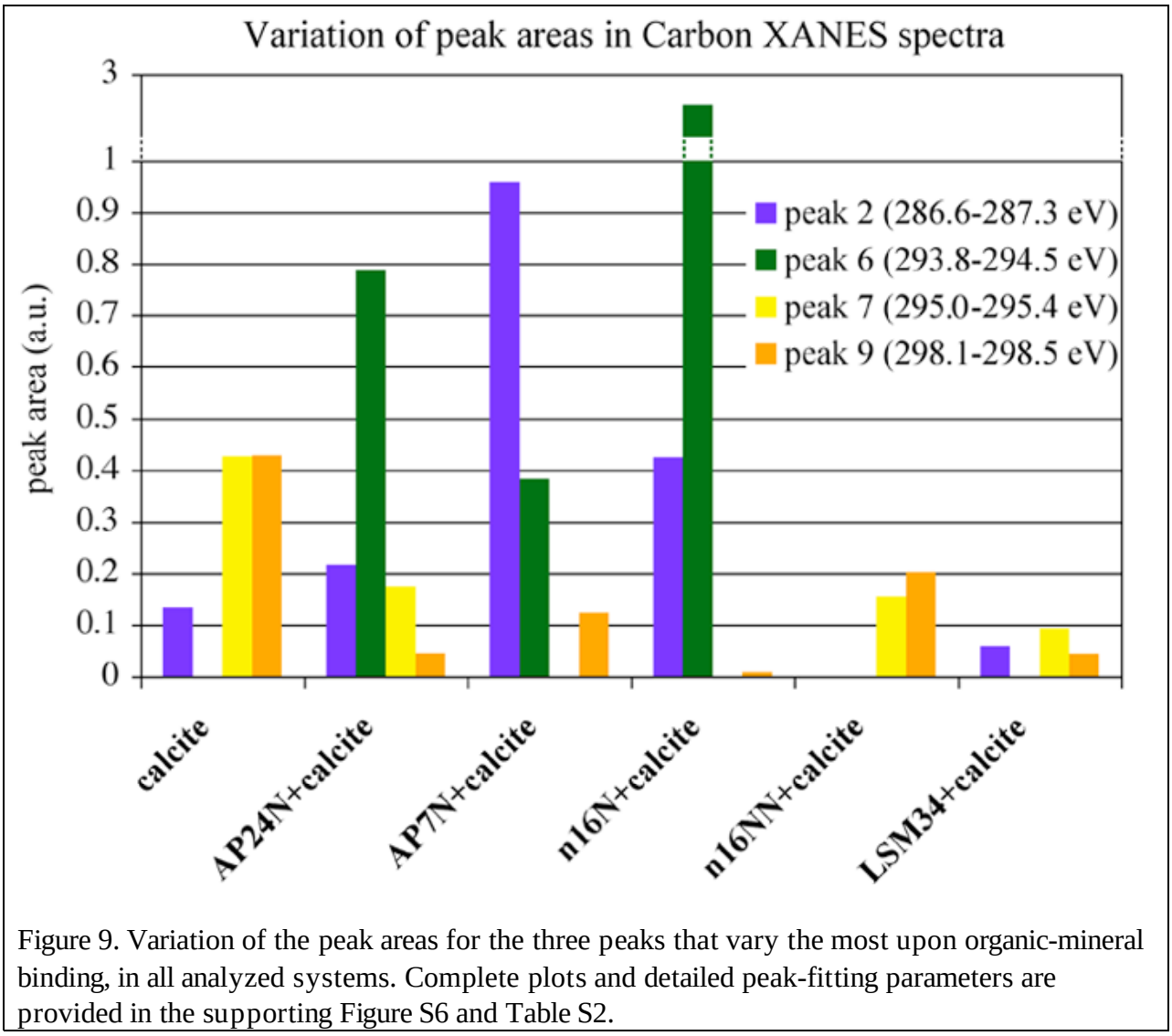

Figure 9. Variation of the peak areas for the three peaks that vary the most upon organic-mineral binding, in all analyzed systems. Complete plots and detailed peak-fitting parameters are provided in the supporting Figure S6 and Table S2.

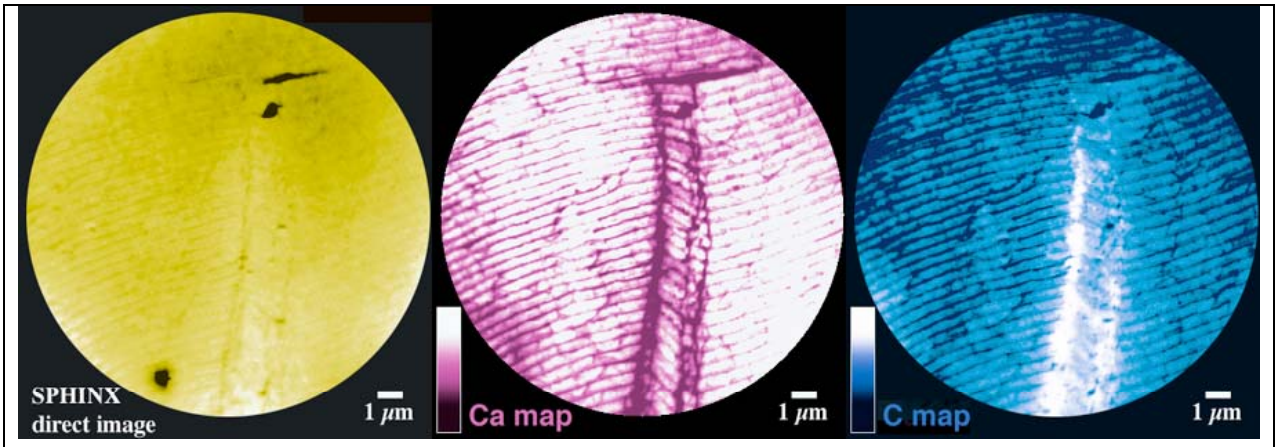

Figure 10. SPHINX image (yellow tritone) and Ca and C distribution maps (magenta and blue tritones) acquired on the polished surface of a cross-section of nacre from red abalone. The nacre layers are interrupted by a crack that the animal healed during its life. The nacre surface and mantle cells were at the bottom right of this field of view, parallel to the nacre layers. Notice the different orientation of the nacre layers in the healed crack compared to the surrounding nacre tissue, and the much larger concentration of carbon (white = high concentration) around the crack edges, which are Ca-poor.